

Effect of Ligand Architecture on the Structure and Properties of Square-Planar Nickel(II) Complexes of Amide-Based Macrocycles

Savita K. Sharma,^[a] Shailesh Upreti,^[b] and Rajeev Gupta^{*[a]}

Keywords: Nickel complexes / Macrocyclic ligands / Electrochemistry

The present work discusses the design and synthesis of four novel macrocyclic ligands and their Ni^{II} complexes. All four ligands (H₂1^{EN}, H₂2^{EN}, H₂3^{OP}, H₂4^{OP}) are designed to provide an identical donor-environment composed of two deprotonated anionic amide-*N* coordination and two neutral amine-*N* coordination and an identical 12-membered macrocyclic ring around the nickel center. The Ni^{II} complexes (**1**, **2**, **3**, and **4** of doubly deprotonated ligands [1^{EN}]²⁻, [2^{EN}]²⁻, [3^{OP}]²⁻, and [4^{OP}]²⁻, respectively) are prepared and thoroughly characterized. The coordination geometry around the Ni^{II} center is square planar as determined by the single crystal structure analyses. The average Ni–N_{amide} bond lengths are shorter by ca. 0.1 Å than the average Ni–N_{amine} distances while the average N_{amide}–Ni–N_{amide} angles are shorter by ca. 4° than the average N_{amine}–Ni–N_{amine} angles. The Ni^{II} ion is housed quite tightly within the aperture of the macrocycle as seen by the short Ni–N bond lengths and a very small

displacement (0.11–0.17 Å) of the Ni center out of the N₄ basal plane. The detailed ¹H and ¹³C NMR studies on the diamagnetic Ni-complexes reveal that the solid state conformation of the complexes **1–4** is retained in the solution. The Ni^{III/II} potential is fairly positive (>0.6 V vs. SCE) for all four complexes, while the complexes with phenylene as part of the ligand also show the oxidation(s) of the ring(s) (>1.1 V vs. SCE). Coulometric measurements confirm both responses as 1e⁻ process. Electrochemical or chemical oxidation at the 1st potential results in the generation of an unstable “green species” that show distinct features in the absorption spectrum and exhibit anisotropic EPR spectrum. These findings strongly point out that the unstable green species is a Ni^{III} species. The 2nd and/or 3rd oxidation is centered on the phenylene ring(s) and lead to an immediate decomposition. (© Wiley-VCH Verlag GmbH & Co. KGaA, 69451 Weinheim, Germany, 2007)

Introduction

The interest in the nickel coordination complexes supported with amide ligands has always attracted synthetic chemists due to many reasons. One of them is to stabilize nickel ions in high oxidation states to gain knowledge about such species in general and to further use them as oxidizing agents.^[1] Secondly, the recent developments in spectroscopic and/or structural identification of the nickel species in the catalytic cycle of several enzymes, for example, [NiFe]-hydrogenases,^[2] Ni-dependent superoxide dismutase,^[3] acetyl-coenzyme A synthase^[4] and Ni-tetrahydrocorphinoid cofactor (F₄₃₀) of methyl-coenzyme M reductase^[5] has reignited the interests in the area of bioinorganic model studies of nickel ion. In fact, the identification of deprotonated carboxamido-*N* coordination in a number of Ni-enzymes has challenged the synthetic chemists to design the low-molecular weight models to understand the structure

and function of the native enzymes. A latest case is the emergence of quite interesting synthetic systems to model the active site structure of Acetyl coenzyme A synthase/carbon monoxide dehydrogenase (ACS/CODH).^[6] Also, Ni^{II} in conjunction with oligopeptides has found to cause DNA cleavage in the presence of suitable oxidants; Ni^{III} and/or Ni^{IV} species have been postulated for this cleavage.^[7] In this context, as well as in order to develop better oxidizing systems, emphasis should be to achieve a higher oxidation state of the nickel ion. The redox properties of a nickel center can be fine-tuned by the use of strong donor groups in a constrained environment in conjunction with the incorporation of non-innocent ligand features that also participate in the redox properties.

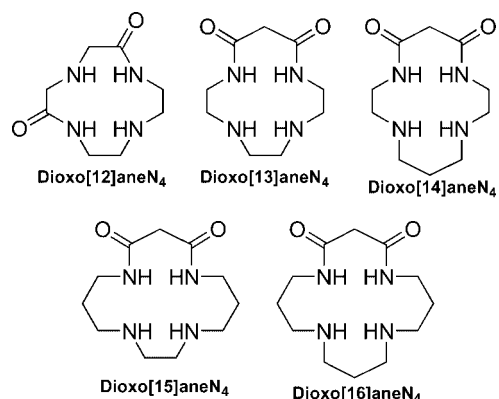
Amide-based macrocyclic ligands possess interesting oligopeptide features of the biologically important moieties and serve as effective ligands for early and late transition metal ions.^[8,9] Extensive research has been devoted in understanding the nickel coordination chemistry with amide-based azamacrocyclic ligands;^[8] however, studies have mainly been limited to the solution generated species in most of the instances with structural information limited to handful examples. Such studies have primarily been targeted to understand the effective placement of the nickel ion within the aperture or the cavity of the macrocycle with

[a] Department of Chemistry, University of Delhi, Delhi 110007, India
Fax: +91-11-2766-6605
E-mail: rgupta@chemistry.du.ac.in

[b] Department of Chemistry, Indian Institute of Technology, Delhi, New Delhi, 110016, India

Supporting information for this article is available on the WWW under <http://www.eurjic.org> or from the author.

the emphasis on the 13- and 14-membered dioxotetraamines (see Scheme 1). The pioneering work of Kimura and Kodama^[10] has resulted in a number of important conclusions, for example, 13-membered macrocycle, dioxo[13]aneN₄ ideally house the low-spin Ni^{II} ion tightly compared to the analogous 14-membered, dioxo[14]aneN₄ and 15-membered, dioxo[15]aneN₄ macrocycles. In continuation, they also show that the macrocyclic ring size (13...15-membered) has a profound effect on the redox potential of the Ni^{II}/Ni^{III} couple. Lampeka and Gavriush^[11,12] have further progressed this work and recently shown the crystal structures of the Ni^{II} complexes with dioxo[13]aneN₄ and dioxo[14]aneN₄ ligands. Both Ni complexes, as anticipated earlier, are square planar and the solid-state structures have shown to be retained in solution by the proton NMR studies. In spite of the importance anticipated for the 12-membered macrocycles (such as small size of the macrocyclic aperture and tight chelation), surprisingly, the chemistry has not been explored. A possible explanation for the expansion of the chemistry of 13-membered or higher macrocycle is the readily accessibility of such ligands via the aminolysis reaction of malonic esters with variable polyamines.^[8] Moreover, it was always anticipated that a tiny 12-membered macrocycle may not be able to accommodate a transition metal ion. In fact, Martell and co-workers^[13] have shown few 2:1 sandwich metal complexes of a very similar amide ligand (1,4,7,10-tetraazacyclododecane-2,9-dione), where M^{II} (M = Co, Ni, and Cu) ion is in between two ligands. This is to be noted, however, that these complexes were synthesized and isolated at neutral pH. These literature precedents have laid the foundation of our present work and we have commenced a systematic synthetic investigation to shed light on the effect of the ligand architecture imposed by the macrocyclic ligands on the properties of coordination complexes. Herein, we report the design and synthesis of four novel macrocyclic ligands and their coordination chemistry towards Ni^{II} ion. These ligands have been designed to keep two important parameters identical; basic donor-environment around the nickel center, and the size of macrocycle which is 12-membered in all four cases. This is followed by the understanding of the effect of ligand planarity and non-innocent feature(s) on the structural, spectroscopic, and redox properties of the nickel center.

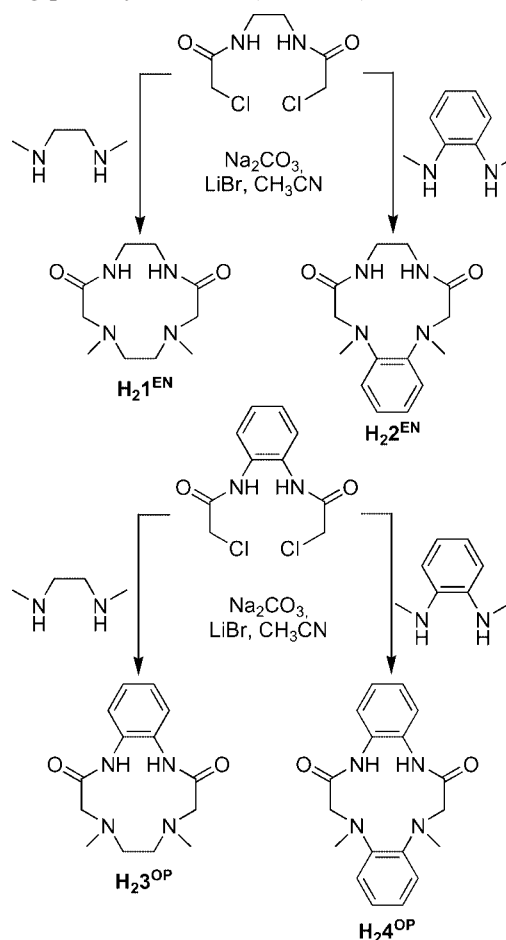


Scheme 1.

Results and Discussion

Ligand Design and Synthesis

The macrocyclic ligands (H₂1^{EN}, H₂2^{EN}, H₂3^{OP}, and H₂4^{OP}) are designed to simultaneously provide two amide and two amine coordinations to the metal center. Moreover, the ligands are intended to afford an identical primary coordination environment to the metal center. The only difference between these four ligands is the subtle alteration in the backbone of the ligands. For example, H₂2^{EN} differ from H₂1^{EN} by the involvement of one phenylene unit in the framework of the macrocycle, whereas H₂4^{OP} differ from H₂1^{EN} by the incorporation of two such units. These ligands are synthesized in two steps starting from the corresponding primary diamines (Scheme 2).



Scheme 2. Synthesis of ligands.

In the first step, the diamine is converted into the respective bis(chloroacetamide) by treating with two equiv. of chloroacetyl chloride.^[14] In the next step, the bis(chloroacetamide) is treated with the corresponding secondary amine to afford the desired ligand. It is worth mentioning here that during the synthesis of these ligands, LiBr was used as a templating agent.^[15] Interestingly, the synthetic attempts were unsuccessful without the addition of LiBr as templating agent. The utilization of a templating agent is well known in the literature for the synthesis of macrocyclic

ligands from simple crown-ethers to more complex molecules.^[16] All new ligands are thoroughly characterized using various spectroscopic measurements and give satisfactory microanalysis results.

Synthesis and Characterization of Metal Complexes

All Ni^{II} complexes, **1–4**, were synthesized as follows: DMF solution of the respective ligand was first deprotonated with solid NaH under N₂ atmosphere followed by the addition of NiCl₂ as the metal source. The complex **1** can, however, be synthesized in better yield by treating the methanolic solution of the ligand H₂L^{EN} with 2 equiv. of NaOH followed by the addition of the Ni(OAc)₂ salt. Usual workup and recrystallization (vapor diffusion of diethyl ether to a MeCN solution of complexes) afforded highly crystalline material in moderate recrystallized yield (ca. 40%). All complexes are deep yellow to orange-yellow in color.

In the FTIR spectra, the absence of $\nu(\text{N-H})$ stretching frequency confirms the deprotonated nature of the amide ligands. A bathochromic shift in the C=O stretching frequency was observed for all complexes compared to the free ligand and prove that the deprotonated N-amide group is coordinated to the Ni ion.^[17] In addition, complex **2** also has water as solvent of crystallization which shows the $\nu(\text{OH})$ ^[17] absorption in the region of 3300–3400 cm⁻¹ (cf. crystal structure). Solution conductivity data^[18] confirm the non-electrolytic nature of all Ni^{II} complexes, whereas the elemental analyses results authenticate the purity of the bulk samples. In the electrospray mass spectra, molecular ion peak corresponding to the complexes, **1**, **2**, **3**, and **4** were obtained at 285.05 (**1** + H⁺), 333.27 (**2** + H⁺), 333.05 (**3** + H⁺), and 381.35 (**4** + H⁺), respectively, and assert the integrity of the metal complexes in the solution.

Crystal Structure Studies

All Ni^{II} complexes have been structurally characterized and the molecular structures of the complexes are shown in Figures 1, 2, 3, and 4, while the important crystallographic

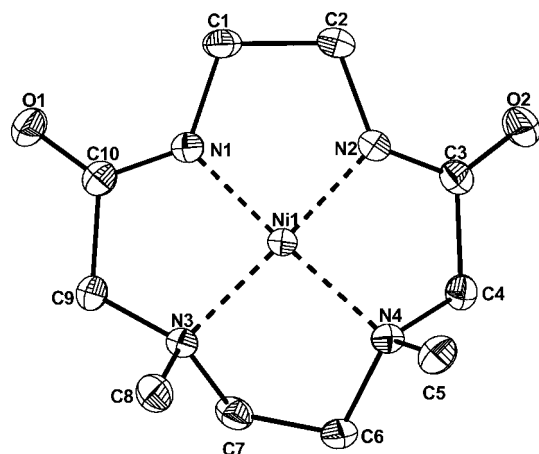


Figure 1. Molecular structure of complex **1** (thermal ellipsoid are drawn at 30% probability level). Hydrogen atoms, solvent molecule are omitted for clarity.

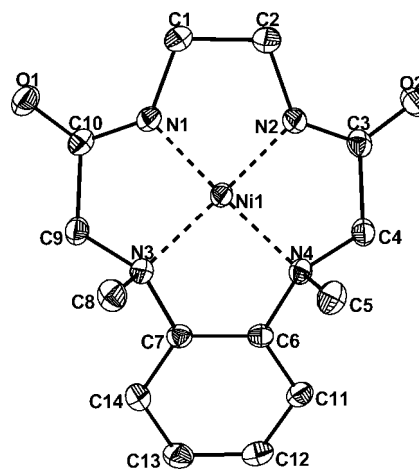


Figure 2. Molecular structure of complex **2** (thermal ellipsoid are drawn at 30% probability level). Hydrogen atoms, solvent molecule are omitted for clarity.

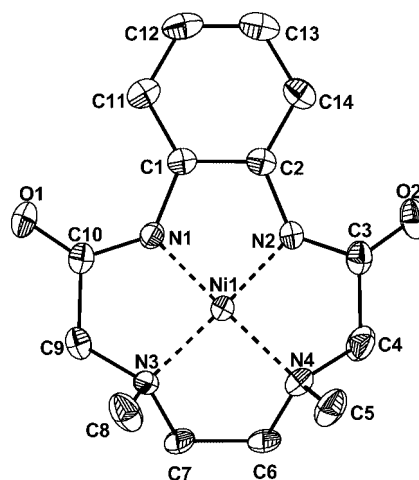


Figure 3. Molecular structure of complex **3** (thermal ellipsoid are drawn at 30% probability level). Hydrogen atoms are omitted for clarity. The atoms C6 and C7 were occupying two crystallographically independent positions and only the atoms with site occupancy factor of 0.8 are shown for clarity.

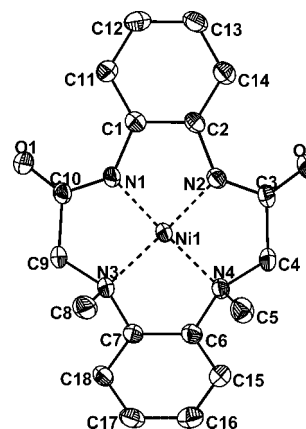


Figure 4. Molecular structure of complex **4** (thermal ellipsoid are drawn at 30% probability level). Hydrogen atoms are omitted for clarity.

and structural parameters are presented in Tables 1, 2 and S1 (for the latter see electronic supporting information). The coordination geometry around the Ni^{II} center is square planar in all four complexes. The Ni^{II} ion is simultaneously coordinated by two deprotonated amidic-*N* atoms and two tertiary amine-*N* atoms. In all four complexes Ni^{II} ion is surrounded by four five-membered chelate rings. In all cases, the bond angles formed by the lateral chelate rings about the Ni center are close to the ideal value of 90° for a perfect square-planar complex; however, the bond angle involving two anionic N_{amide} has a slightly smaller value of ca. 88° which is compensated by a little higher angle (ca. 92°) for the chelate ring involving two N_{amine}. The methyl groups on the tertiary nitrogen centers are located on one side of the plane in all cases. This is in contrast to a number of examples where relative position of the N–H or N–R groups results in the occurrence of the geometrical isomers.^[11] The lateral 5-membered chelate rings [–C(O)–CH₂– fragment] in all complexes are adopting the envelope con-

formation.^[11,19] Both carbon atoms in these rings are present on the same side of N_{amide}–Ni–N_{amine} plane with larger displacement of the carbon atoms connected to the amine nitrogens (sp³ centers).

For complex **1**, the average Ni–N_{amide} bond length is ca. 1.81 Å, while the average Ni–N_{amine} bond length is ca. 1.91 Å. The difference of 0.1 Å may be attributed to the anionic coordination from the deprotonated amidic nitrogens compared to the neutral amine nitrogen donors. The N(1)–Ni–N(2) bond angle of 87.40° is smaller than the N(3)–Ni–N(4) bond angle of 92.36°. The observed difference of ca. 5° between the two bond angles explains the tight chelate formation from the two anionic amidate nitrogens. The other two angles (ca. 89°) involving lateral five-membered rings are similar to each other. Another interesting feature of the structure is the orientation of the carbon centers of the –CH₂CH₂– fragments of the amine part of the macrocyclic ligand which is adapting *gauche* conformation.^[11]

Table 1. Crystallographic data for [Ni(1^{EN})] (**1**), [Ni(2^{EN})] (**2**), [Ni(3^{OP})] (**3**), and [Ni(4^{OP})] (**4**).

Complex	[Ni ^{II} (1 ^{EN})] (1 ·CH ₃ CN)	[Ni ^{II} (2 ^{EN})] (2 ·H ₂ O)	[Ni ^{II} (3 ^{OP})] (3)	Ni ^{II} (4 ^{OP})] (4)
Empirical formula	C ₁₂ H ₂₁ N ₅ O ₂ Ni	C ₁₄ H ₂₀ N ₄ O ₃ Ni	C ₁₄ H ₁₈ N ₄ O ₂ Ni	C ₁₈ H ₁₈ N ₄ O ₂ Ni
Formula mass	326.03	351.03	333.01	381.05
<i>T</i> [K]	298	298	298	298
Crystal system	triclinic	orthorhombic	monoclinic	triclinic
Space group	<i>P</i> $\bar{1}$	<i>P</i> 2 ₁ 2 ₁	<i>P</i> 2 ₁ / <i>n</i>	<i>P</i> $\bar{1}$
Color, shape	yellow, needle	yellow, plate	yellow, block	yellow, block
<i>a</i> [Å]	8.684(3)	8.998(8)	8.9315(9)	11.676(3)
<i>b</i> [Å]	9.095(5)	10.562(2)	10.319(1)	11.739(4)
<i>c</i> [Å]	9.449(7)	16.411(3)	15.502(6)	13.271(5)
α [°]	100.771(2)			78.597(4)
β [°]	98.061(3)		101.237(2)	69.901(5)
γ [°]	92.061(2)			80.854(6)
<i>V</i> [Å ³]	724.4(7)	1559.7(14)	1401.3(6)	1666.3(10)
<i>Z</i>	2	4	4	4
<i>D</i> _{calcd.} [g cm ^{−3}]	1.495	1.496	1.578	1.515
Absorption coefficient [mm ^{−1}]	1.348	1.262	1.394	1.184
<i>R</i> ^[a]	0.0386	0.0244	0.0403	0.0520
<i>R</i> _w ^[b]	0.0874	0.0601	0.1003	0.1415
GOF on <i>F</i> ²	1.000	1.072	1.132	1.139

[a] $R = \sum ||F_o| - |F_c|| / \sum |F_o|$. [b] $R_w = \{[\sum (|F_o|^2 - |F_c|^2)^2]^{1/2}\}^{1/2}$.

Table 2. Selected bond lengths and angles for [Ni(1^{EN})] (**1**), [Ni(2^{EN})] (**2**), [Ni(3^{OP})] (**3**), and [Ni(4^{OP})] (**4**).

Bond length	[Ni ^{II} (1 ^{EN})] (1)	[Ni ^{II} (2 ^{EN})] (2)	[Ni ^{II} (3 ^{OP})] (3)	[Ni ^{II} (4 ^{OP})] (4) ^[a]
Ni1–N1	1.806(3)	1.822(4)	1.801(2)	1.812(4), 1.824(4)
Ni1–N2	1.808(3)	1.813(3)	1.805(2)	1.803(4), 1.817(4)
Ni1–N3	1.904(2)	1.910(3)	1.889(2)	1.901(4), 1.896(4)
Ni1–N4	1.908(3)	1.910(4)	1.890(2)	1.896(4), 1.897(4)
C3–O2	1.232(4)	1.260(3)	1.224(4)	1.232(6), 1.230(6)
C10–O1	1.232(4)	1.253(3)	1.227(4)	1.229(6), 1.237(5)
Bond angles				
N1–Ni1–N2	87.40(11)	87.90(12)	87.24(10)	87.33(18), 87.60(17)
N3–Ni1–N4	92.36(11)	92.08(12)	92.44(11)	92.00(17), 91.89(16)
N1–Ni1–N3	89.57(11)	89.76(12)	89.65(11)	89.90(17), 89.47(16)
N2–Ni1–N4	88.83(11)	89.05(12)	89.86(10)	89.71(18), 89.78(17)
N1–Ni1–N4	171.31(12)	170.43(9)	172.09(11)	171.97(17), 169.59(16)
N2–Ni1–N3	166.93(11)	172.31(7)	173.26(11)	171.76(18), 172.51(16)

[a] There are two independent molecules in the asymmetric unit cell. Metric parameters are reported for both independent molecules.

The average Ni–N_{amide} and Ni–N_{amine} distances at ca. 1.81 Å and 1.91 Å, respectively, for complex **2** are identical to **1**. The other distances and angles are comparable to that of **1**. However, the amine carbon centers emerging from the 1, 2-diaminobenzene are now planar as a result of the involvement of a rigid phenylene unit. Interestingly the carbon centers of the –CH₂CH₂– fragments connected to the amide part of the macrocyclic ligand are now adopting a partial *gauche* conformation.^[11] Moreover, the unit cell has a water molecule which is hydrogen bonded to the amide oxygen atoms from two different molecules of **2**. The consequence is the formation of a zig-zag chain with alternate arrangement of complex **2** and H₂O (Figure S1).

The average bond lengths for **3** are similar to that of **1** and **2**. The –CH₂CH₂– fragment of the amine part is now adopting envelope conformation^[11,19] in contrast to the *gauche* conformation of **1**. Moreover, the incorporation of the phenylene group as part of the macrocyclic backbone resulted in a more planar arrangement of the chelate involving two amidic nitrogens than in case of **1** and **2** (cf. Table S1).

In line with other three complexes, the bond lengths and angles for the complex **4** are also comparable. Interestingly, due to the involvement of the phenylene groups both from the amide part of the macrocyclic backbone as well as the amine part of the macrocyclic backbone, the attached carbon centers have become co-planar as can be seen by their respective angles. However, the molecule as a whole is non-planar and adopts a saucer shaped conformation (lateral view, Figure S2).

The average Ni–N_{amide} bond lengths of the present complexes are shortest among the reported examples having a similar coordination environment.^[10f,10g,11,12] For example, the average Ni–N_{amide} bond lengths for the Ni^{II} complexes of the ligands, dioxo[13]aneN₄ and dioxo[14]aneN₄ are 1.839 and 1.889 Å, respectively.^[11] In fact, the average Ni–N_{amide} bond lengths distance of the complexes reported in this work are 0.04–0.05 Å shorter than the mentioned examples. This is worth to mention here that the average Ni–N_{amide} bond lengths of a Ni^{III} complex of a tetraamide ligand of Collins^[20] is ca. 1.84 Å which is 0.04 Å longer than our complexes.

The deviation of the Ni^{II} ion from the coordination basal plane (defined by N1, N2, N3, and N4) is an indication of the optimal placement of the metal ion within the macrocyclic aperture. This out of N₄ basal plane displacement is maximum for the **1** (0.170 Å) and minimum for the **4** (0.110 Å) with other two complexes **2** and **3** have intermediate values. These numbers suggest that the Ni²⁺ ion is most tightly and optimally placed in **4** (Table S1).

The angles between the various planes are presented in Table S1. In general, the plane involving N_{amide} centers (N1 and N2) are comparatively planar due to the enhanced delocalization in the amide fragment. The angle between the plane comprising both N_{amide} (Ni1, N1, C1, C2, and N2) and the plane involving both N_{amine} (Ni1, N4, C6, C7, and N3) is quite significant. This value varies from 23.62° to 28.70° in all four cases and explains the reason for a saucer-

shaped structure of the complexes (lateral view, Figure S2). Similarly, the angle between planes involving lateral carbon centers varies from 30.27° for **3** to 40.29° for **1** and points out towards the envelope conformation.

Absorption Spectral Studies

The absorption spectra of **1–4** complexes in MeCN are displayed in Figure 5. All complexes are deep yellow in color and their absorption spectra display distinct features for the four-coordinate square planar Ni^{II} ion. Complexes **1–4**, display the λ_{max} within a small range of 436 to 444 nm, thus indicating a similar electronic environment created by the ligand around the Ni ion. The observed similarity between the absorption features of complexes is also reflected in their very similar solid state crystal structures (vide supra) as well as NMR spectra (vide infra). High energy features are observed below 310 nm and could tentatively be assigned as intra-ligand transitions. The absorption spectral features of Ni^{II} complexes of macrocyclic ligands have been subjected to detailed investigations to understand the ligand planarity and the placement of the Ni center in the cavity of the macrocycle.^[8,10a,21] It has been suggested that the lower the λ_{max} value for the Ni^{II} complex better the fitting of the Ni^{II} center inside the macrocyclic cavity. Comparing the λ_{max} values of the Ni^{II} complexes, it is clear that the complexes **1** and **2** differ marginally with each other, while the complexes **3** and **4** indicate an almost identical placement. These data indicate that in the solution state the Ni^{II} ion is most optimally placed within the basal plane provided by the ligand framework in the following order: **1**, **2**, **3** \approx **4**.

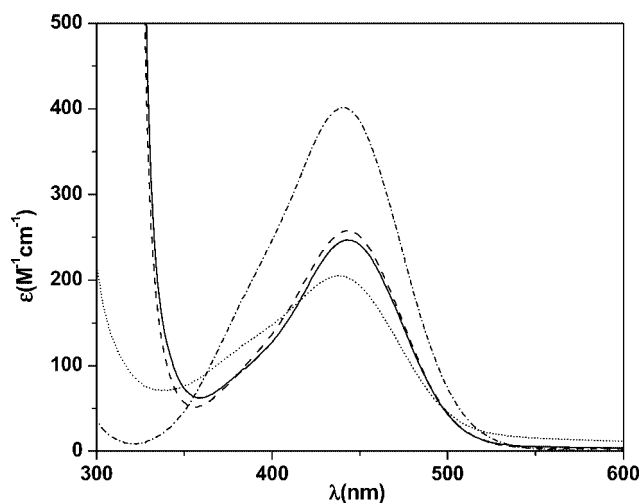


Figure 5. UV/Vis spectra of Ni^{II} complexes in CH₃CN: complex **1** (– · – · – ·), complex **2** (—), complex **3** (---), and complex **4** (.....).

In order to analyze the binding affinity of the axial ligands towards the present square planar Ni^{II} complexes, **1–4** were titrated with few potential monodentate ligands [Cl[–], pyridine, 4-(dimethylamino)pyridine]. No change in the absorbance maximum was observed for any of the four complexes. This experiment rules out the binding affinity of

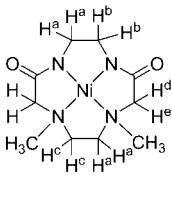
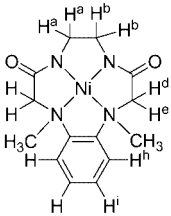
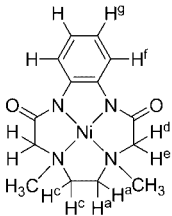
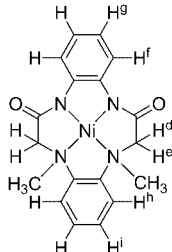
such ligands towards nickel complexes. For the similar reason, absorption spectra were also recorded in better coordinating solvent, for example, DMF, DMSO, and H₂O (Figure S3, S4, and S5). The λ_{max} was observed in a narrow range (430–444 nm) for all four complexes, thus again eliminates the possibility of the solvent coordination. A shoulder at ca. 380 nm was also noticed for all complexes; the intensity of this shoulder was found to vary with the solvent of study.

Nuclear Magnetic Resonance Studies

To investigate the solution state structures of the nickel complexes, their ¹H and ¹³C NMR spectroscopic studies were performed (Figures S6, S7, S8, S9 and Table 3, Table S2). ¹H NMR spectra of all complexes were recorded in [D₆]DMSO as well as in CD₃CN and are very similar. All complexes, **1–4** are diamagnetic with *S* = 0 ground state as displayed by their diamagnetic NMR spectra. Assignments of the signals have been made through the consideration of the relative peak areas and comparison with free ligand spectrum. However, in the case of complex **1**, 2D {¹H-¹³C} correlation spectrum was also performed to accurately assign various signals (Figure S10). The ¹H NMR spectra of all complexes are quite interesting and deserve special attention. The twisting of the –CH₂CH₂– fragment (of the *N,N'*-dimethylethylenediamine part) results in the different chem-

ical environment of the protons attached to these carbon centers. Two sets of H signals were observed as multiplets for complex **1** and **3** at 2.67 and 3.76; and 2.74 and 3.86 ppm, respectively (labeled as proton *a* and *c*, respectively). The –CH₂CH₂– fragment of the deprotonated amide backbone was also twisted and resulted in the appearance of the multiplets at δ = 2.67 and 3.21 ppm (labeled as proton *a* and *b*, respectively) for **1**, and 2.78 and 3.22 ppm for **2**, respectively. Coincidentally, for complex **1**, one of the –CH₂– group's proton signals (labeled as proton *a*) were observed at the same position suggesting a similar chemical environment. The most interesting aspect of the spectra of all complexes **1–4** is the observation of the AB-type coupling (or geminal coupling) between the protons attached to the –C(O)CH₂– fragment.^[11,12] The signals for the pair of protons from the –C(O)CH₂– fragment (*d* and *e*) appear at δ = 3.07 and 4.00 ppm for **1**, 3.70 and 4.15 for **2**, 3.12 and 4.13 ppm for **3**, and 3.89 and 4.43 ppm for **4**. The geminal coupling constant, *J*(*H^dH^e*) for complexes **1** and **3** was 15.9 Hz, while a value of ca. 15.5 Hz was observed for **2** and **4**, respectively. The observation of the AB-type coupling in these complexes suggests the rigid nature of the macrocyclic ligands that places protons *d* and *e* in different chemical environment. In general, the ¹H NMR spectra of the transition metal complexes of azamacrocyclic ligands are complicated due to the “frozen” conformation of the chelate rings^[11,12] and the spectra of **1**, **2**, **3**, and **4**

Table 3. ¹H NMR data of [Ni^{II}(1^{EN})] (**1**), [Ni^{II}(2^{EN})] (**2**), [Ni^{II}(3^{OP})] (**3**), and [Ni^{II}(4^{OP})] (**4**).^[a]

Proton	[Ni ^{II} (1 ^{EN})] (1)	[Ni ^{II} (2 ^{EN})] (2)	[Ni ^{II} (3 ^{OP})] (3)	[Ni ^{II} (4 ^{OP})] (4)
				
a	2.67, m (2.66, m)	2.78, m (2.73, m)	2.74, m (2.80, m)	–
b	3.21, m (3.25, m)	3.22, m (3.23, m)	–	–
c	3.76, m (3.69, m)	–	3.86, m (3.89, m)	–
d	3.07, d, <i>J</i> = 15.9 ^[b] (3.08, d, <i>J</i> = 15.9 ^[b])	3.70, d, <i>J</i> = 15.5 ^[b] (3.58, d, <i>J</i> = 15.6 ^[b])	3.12, d, <i>J</i> = 15.9 ^[b] (3.28, d, <i>J</i> = 16.2 ^[b])	3.89, d, <i>J</i> = 15.5 ^[b] (3.80, d, <i>J</i> = 15.3 ^[b]) [3.86, d, <i>J</i> = 15.14 ^[b]]
e	4.00, d, <i>J</i> = 15.9 ^[b] (3.90, d, <i>J</i> = 15.9 ^[b])	4.15, d, <i>J</i> = 15.5 ^[b] (4.13, d, <i>J</i> = 15.3 ^[b])	4.13, d, <i>J</i> = 15.9 ^[b] (4.14, d, <i>J</i> = 15.9 ^[b])	4.43, d, <i>J</i> = 15.6 ^[b] (4.42, d, <i>J</i> = 15.5 ^[b]) [4.51, d, <i>J</i> = 15.12 ^[b]]
f	–	–	7.41, m (7.56, m)	7.55, m (7.62, m) [7.76, m]
g	–	–	6.54, m (6.70, m)	7.55, m (7.44, m) [7.49, m]
h	–	7.47, m (7.36, m)	–	6.67, m (7.30, m) [7.25, m]
i	–	7.47, m (7.26, m)	–	6.67, m (6.65, m) [6.85, m]
–CH ₃	2.49, s (2.45, s)	2.87, s (2.79, s)	2.52, s (2.64, s)	3.01, s (3.00, s) [3.06, s]

[a] Spectra are recorded in [D₆]DMSO. Parentheses () and square brackets [] indicate values of spectra recorded in CD₃CN and CDCl₃, respectively. Abbreviations: s = singlet; d = doublet; m = multiplet. [b] Geminal coupling constant.

are no exception. Conformational rigidity of such systems results from the fact that the inversion of the chelate rings requires a change of the configuration of the coordinated amine nitrogen atom(s). The complex nature of the ^1H NMR spectra of **1–4** is most likely arising due to the macrocyclic nature of the coordinated ligand. The inherent strain of the macrocyclic ligand have caused few of the carbon centers to be out of the plane as also observed in the crystal structure determination (*vide supra*).

In contrast to the proton NMR spectra, the ^{13}C NMR spectra of **1–4** are quite straight forward (Table S2, Figure S9). Even though proton NMR spectra reflected the complexity arising due to the non-planarity of few carbon centers that resulted in the different chemical environment for the attached protons, the carbon NMR spectra were averaged out. A close similarity in the ^{13}C chemical shifts of identical carbon centers was observed for all complexes. For example, the methyl C signals were observed in a close range of 47–52 ppm. Similarly, the chemical shift for the carbon centers of *N,N'*-dimethylethylenediamine part (labeled as *d*) were seen at $\delta \approx 60$ ppm for **1** and **3**.

There was no evidence of any paramagnetic species in the NMR spectra, which show that the Ni^{II} complexes retain their square-planar geometry in solution. This observation also corroborate the identical conclusion drawn from the absorption spectral studies that the Ni^{II} complexes of the present ligands do not bind various axial ligands [Cl^- , pyridine, 4-(dimethylamino)pyridine, or solvents, etc.].

Electrochemical Studies

Cyclic voltammetric (CV) and controlled potential electrolysis (coulometric) studies were performed for all four Ni^{II} samples to investigate the extent of stabilization of the Ni^{III} state as well as the possible ligand oxidation.^[22] In addition, the CV results will also help in understanding the accessibility of the higher oxidation states and the effect of the ligand architecture on the redox potential. The electrochemical data for complexes **1–4** are summarized in Table 4.

Electrochemistry in CH_3CN

The 1st oxidation process for all complexes is displayed in Figure 6, while the complete oxidation range is shown for complex **4** (Figure 7). In CH_3CN , for 1st oxidation, each complex undergo $1e^-$ oxidation in the potential range of 0.61–0.83 V (vs. SCE). The one electron nature of each redox response has been confirmed by the controlled potential electrolysis experiments. The peak-to-peak separation (ΔE_p) for the 1st response, for complexes **1–4** are in the range of 60–100 mV and point out towards reversible to quasi-reversible nature of the responses (Table 4). For comparison, the redox potential for the complex, $[\text{Ni}(\text{dioxo}[12]\text{-aneN}_4)]$ is 0.62 V^[10b] (vs. SCE in H_2O) while Ni complexes of 13- and 14-analogues appear at higher potential (> 0.80 V, Table 4).^[10b–10e,10g] No reduction wave was observed in the potential range studied (–2.0 V for CH_3CN and –2.2 V for DMF vs. SCE).

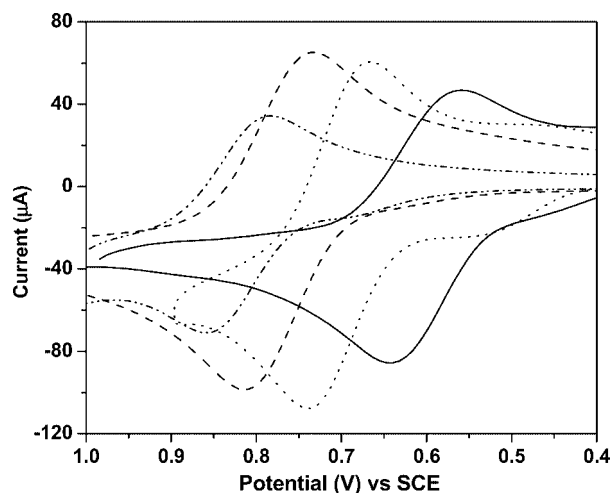


Figure 6. Cyclic voltammograms of Ni^{II} complexes in CH_3CN : complex **1** (—), complex **2** (---), complex **3** (.....), and complex **4** (-.-.-.-).

The complex **1** show only one oxidation response at 0.61 V ($\Delta E_p = 90$ mV), as expected for the Ni^{II} complex of a perfect innocent ligand. On the other hand, rest of the

Table 4. Cyclic voltammetric data^[a] for $[\text{Ni}(\text{1}^{\text{EN}})]$ (**1**), $[\text{Ni}(\text{2}^{\text{EN}})]$ (**2**), $[\text{Ni}(\text{3}^{\text{OP}})]$ (**3**), and $[\text{Ni}(\text{4}^{\text{OP}})]$ (**4**) and comparison with literature examples.

Complex	E_1 [V] in CH_3CN (ΔE_p [mV]); $n^{\text{[c]}}$	E_2 [V] in CH_3CN (E_{pa}); $n^{\text{[c]}}$	E_3 [V] in CH_3CN (E_{pa}); $n^{\text{[c]}}$	E_1 [V] in DMF ^[b] (ΔE_p [mV])	E_2 [V] in DMF ^[b] (E_{pa})	Ref.
$[\text{Ni}(\text{1}^{\text{EN}})]$ (1)	0.61 (90); 0.94	—	—	0.53 (100)	—	this work
$[\text{Ni}(\text{2}^{\text{EN}})]$ (2)	0.78 (100); 0.96	1.88; 1.91	—	0.67 (110)	—	this work
$[\text{Ni}(\text{3}^{\text{OP}})]$ (3)	0.71 (70); 1.00	1.10; 1.98	—	0.67 (80)	1.13	this work
$[\text{Ni}(\text{4}^{\text{OP}})]$ (4)	0.83 (73); 1.02	1.13; 1.96	1.32; 2.9	0.78 (90)	1.20	this work
$[\text{Ni}(\text{dioxo}[12]\text{aneN}_4)]^{\text{[d]}}$	0.62 (100)					[10b]
$[\text{Ni}(\text{dioxo}[13]\text{aneN}_4)]^{\text{[d]}}$	0.90 (80)					[10b,d,e,g]
$[\text{Ni}(\text{dioxo}[14]\text{aneN}_4)]^{\text{[d]}}$	0.80 (80)					[10b,c]
$[\text{Ni}(\text{dioxo}[15]\text{aneN}_4)]^{\text{[d]}}$	0.62 (100)					[10b]

[a] Conditions: Complex ca. 1 mM solution, TBAP as supporting electrolyte as ca. 100 mM solution, potential vs. SCE, glassy carbon as working electrode, Pt as auxiliary electrode, scan rate = 100 mV/s. [b] Pt as working electrode, other conditions are identical. [c] Coulombic n (number of electron(s) taking part in the oxidation process). [d] in water with Na_2SO_4 as supporting electrolyte and glassy carbon as working electrode.

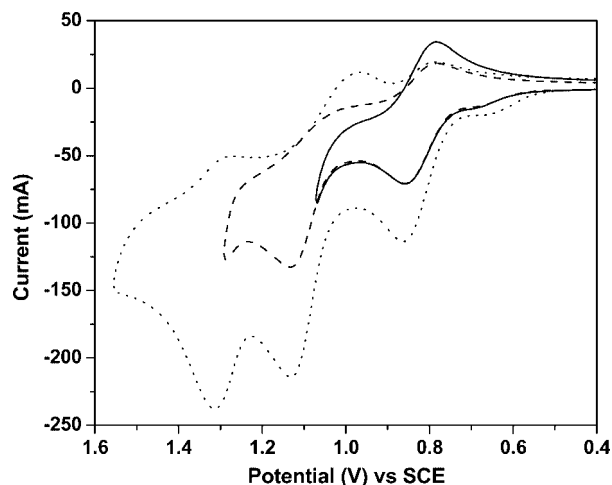


Figure 7. Cyclic voltammogram of complex **4** in CH₃CN.

complexes, **2**, **3**, and **4** display oxidation waves corresponding to both metal as well as the ligand oxidation(s). The extent of the non-innocent feature(s) increases in the following order: **1** > **2** ≈ **3** > **4**. The complex **2** display oxidation waves at 0.78 and 1.88 V (E_{pa}), which we assign as the Ni^{III/II} response and irreversible ligand oxidation, respectively. The similar responses for the complex **3** were observed at 0.71 and 1.1 V (E_{pa}), respectively. For complex **3**, the occurrence of the ligand oxidation potential at much lower potential is most likely due to the involvement of the ring π -current in resonance with the nickel d -electrons. The complex **4** exhibits three oxidation peaks at 0.83 V, 1.13 (E_{pa}), and 1.32 (E_{pa}) V, while the 1st one is metal-centered, the other two processes are ligand-centered. It has been found that the ligands incorporating 1,2-diaminobenzene ring are susceptible to oxidation, generating a cation radical.^[22c,23,24] Based on these literature reports we tentatively assign the redox processes observed at >1.1 V located on the ligand π -system.^[24f,24g]

A comparison of the stepwise redox potential values of the [Ni(Ligand)]^{+/}[Ni(Ligand)] (E_1) and [Ni(Ligand)]^{2+/}[Ni(Ligand)]⁺ (E_2) couples for all four complexes, **1–4** allows the establishment of the nature of the singly, doubly, and in one case triply oxidized species along the present series of the complexes. The four different ligands used in the present study differ only by the placement of the amine and amide fragments within the ethylene or *o*-phenylene part that coordinate to the nickel ion. For example, the ligand H₂**1**^{EN} is an innocent one while the other three ligands have at least one non-innocent feature, either in the form of extended π -conjugated *o*-phenylenediamidate fragment or *N,N'*-dimethyl-*o*-phenylenediamine fragment. The significant shift in the E_1 potentials of complexes **1–4** toward more positive values according to [1^{EN}]²⁻ < [3^{OP}]²⁻ < [2^{EN}]²⁻ < [4^{OP}]²⁻ clearly indicates that the 1st oxidation is metal-centered, leading to a Ni^{III} species. The destabilization of the trivalent oxidation state by increasing the π -conjugated *o*-phenylene fragment(s) is attributed to the poor donor capacity of such ligands due to the delocalization of

the negative charge on the deprotonated amide groups into the attached phenylene fragment.^[25,26]

In contrast, the E_2 value for the second oxidation, for complexes and **3** and **4**, appear at ca. 1.1 V and does not vary upon changing the ligand. This situation is more consistent with ligand-centered oxidation at the *o*-benzenedi-amidate fragment, generating the Ni^{III}-*o*-benzosemiquinone-diimine π -cation species.^[25] The almost identical potential for E_2 (except for complex **2**) rules out metal-centered oxidation as that would have resulted in altered potential due to the ligand field effect. For complex **2**, an irreversible response was observed at a very high potential (ca. 1.9 V vs. SCE). We tentatively assign this response as the oxidation of the *o*-phenylene-*N,N'*-dimethyldiamine fragment. The reason for very high positive potential could be due to the non-conjugation of the sp³-based fragment with Ni center. Interestingly, a 3rd potential (E_3) for the complex **4** was noticed as an irreversible process at ca. 1.3 V vs. SCE. We again assign this redox process based at the *N,N'*-dimethyl-*o*-phenylenediamine fragment. However, why this oxidation appears at a lower potential than the complex **2** is not clear to us.

Electrochemistry in DMF

CV studies were also carried out in DMF to understand the effect of a more polar and better coordinating solvent. A comparative CV plot is shown in Figure 8 while the data are presented in Table 4. As can be seen from the Table 4, the Ni^{III}/Ni^{II} potential are between the range of 0.53 V, lowest for complex **1**, and 0.78 V, highest for complex **4**. A similar trend has been observed before in CH₃CN. However, in general, the Ni^{III} state is more stabilized by 40 mV for complex **3** to 110 mV for **2** in DMF than in MeCN. This investigation reveals that the Ni^{III} state of the complexes is better stabilized due to the enhanced solvation, as the polarity of the solvent increased. Ligand-centered oxidation (E_{pa}) for complexes, **3** and **4** were observed at 1.13 and

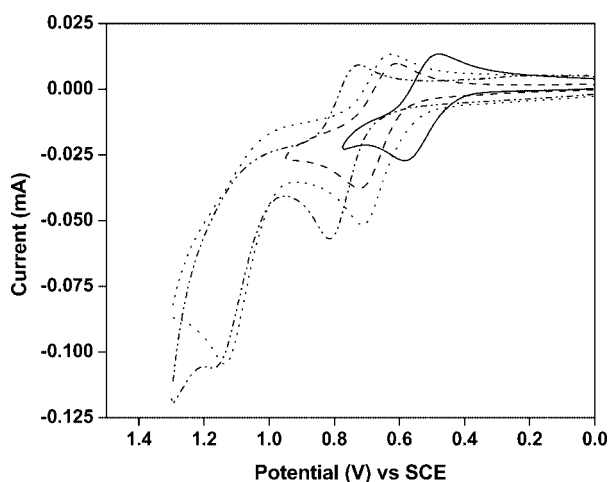


Figure 8. Cyclic voltammograms of Ni^{II} complexes in DMF: complex **1** (—), complex **2** (---), complex **3** (.....), and complex **4** (-.-.-.-).

1.20 V, respectively, as noted before in MeCN. The observed potentials are consistent with the oxidation of *o*-benzenediamide fragment, generating the Ni^{III} -*o*-benzosemiquinonediimine π -cation species. Finally, the oxidation of the *N,N'*-dimethyl-*o*-phenylenediamine fragment was not observed within the solvent limit.

Electrochemical Oxidation and Spectroscopic Characterization of the Oxidized Species

The singly oxidized forms of complexes, **1–4** were generated electrochemically in CH_3CN solution and characterized by the absorption and EPR spectroscopy. The electrochemical oxidation of the solution containing the respective Ni^{II} complex generated a metastable green to greenish-brown species which was stable enough to record the absorption (Figure 9) and the EPR spectra (Figure 10).

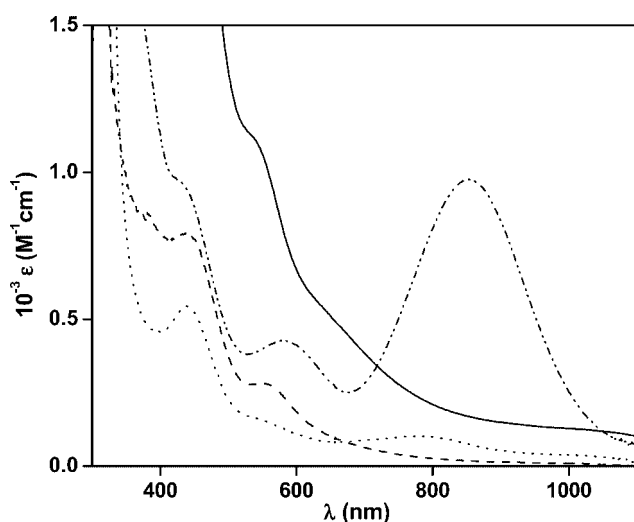


Figure 9. Absorption spectra of electrochemically generated $[1^{\text{Ox}}]^+$, $[2^{\text{Ox}}]^+$, $[3^{\text{Ox}}]^+$, and $[4^{\text{Ox}}]^+$ in CH_3CN : complex $[1^{\text{Ox}}]^+$ (—), complex $[2^{\text{Ox}}]^+$ (---), complex $[3^{\text{Ox}}]^+$ (-·-·-), and complex $[4^{\text{Ox}}]^+$ (·····).

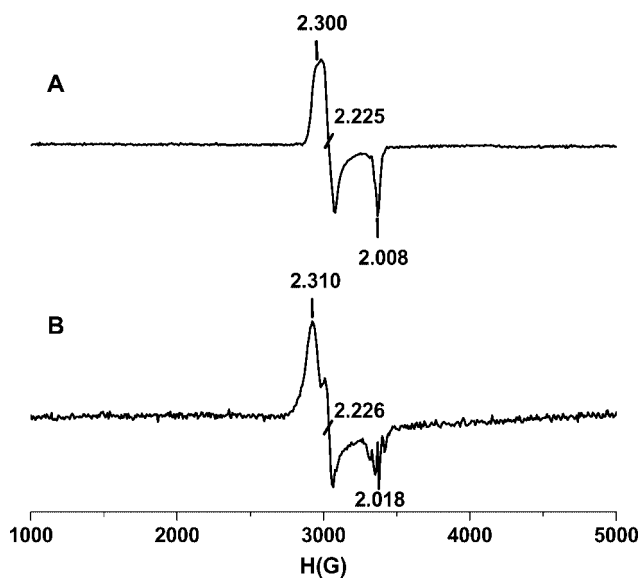


Figure 10. EPR spectra of electrochemically generated $[2^{\text{Ox}}]^+$ (A) and $[3^{\text{Ox}}]^+$ (B) species in CH_3CN at 100 K.

The absorption spectra of these oxidized complexes have rich features and are dominated by a string of charge-transfer bands having ϵ values in the range of $200\text{--}1000\text{ M}^{-1}\text{ cm}^{-1}$. For complex **1**, the oxidized species $[1^{\text{Ox}}]^+$ was generated after oxidizing the solution at 0.8 V vs. SCE and resulted in a brownish-green colored solution. This solution displays broad features at ca. 1000, ca. 660 and ca. 540 nm and justifies its brownish-green color. The $[2^{\text{Ox}}]^+$ was generated after setting the potential at 0.95 V vs. SCE and produced a green solution with λ_{max} at 555 and 437 nm. An intense deep green solution resulted when the complex **3** was oxidized at 0.90 V. Here, an exceptionally intense peak with λ_{max} at 855 nm (ϵ ca. $1000\text{ M}^{-1}\text{ cm}^{-1}$) was noticed along with two weak features at 580 and ca. 430 nm. Qualitatively, this oxidized species was also the most stable one. We believe that the close proximity of the *o*-benzenediamide fragment with the Ni^{III} center has helped in the delocalization of the unpaired spin onto the ligand's π orbitals. This enhanced delocalization has resulted in the better stability of the green species as well as the occurrence of the intense and broad absorption features in the visible region. In contrast, a less stable pale-green species resulted after the oxidation at 1.0 V for complex **4**. For $[4^{\text{Ox}}]^+$, the absorption features were observed at ca. 1020, 780, ca. 550, and 440 nm. By a purely qualitative comparison, the oxidized species $[2^{\text{Ox}}]^+$ and $[4^{\text{Ox}}]^+$ are more unstable than the other two species, $[1^{\text{Ox}}]^+$ and $[3^{\text{Ox}}]^+$. The most probable reason is that the incorporation of the non-planar *N,N'*-dimethyl-*o*-phenylenediamine fragment in the complexes, **2** and **4** (cf. crystal structures) may have increased the distortion at the nickel center and diminish the possibility of the delocalization of the unpaired spin accumulated on the Ni^{III} ion.

The Ni^{II} complexes of various macrocyclic ligands listed in Scheme 1 have also been reported for their ability to stabilize the Ni^{III} state. The electrochemical or chemical oxidation of the aqueous solution resulted in the generation of a “brown” species that displays transitions in the UV region, 300–360 nm.^[10b,10d,27,28] The nature of these transitions has been suggested to be charge transfer. A six-coordinate species has been suggested with solvent molecules serving as the axial ligands. Recently, Journaux and Garcia have reported a solution generated Ni^{III} species of a tetradentate tetraamide ligand.^[25c] For this systems, the λ_{max} for the Ni^{III} species was observed at 910 with a shoulder at 760 nm. The observed similarity between the Ni^{III} species of Journaux and Garcia to that of our systems suggest a similar electronic chromophore.^[25c]

The solution generated oxidized species, $[1^{\text{Ox}}]^+ - [4^{\text{Ox}}]^+$, display anisotropic signals in their X-band EPR spectra. The EPR spectra of the singly oxidized Ni^{III} -complexes, $[2^{\text{Ox}}]^+$ and $[3^{\text{Ox}}]^+$ in the frozen CH_3CN solution at 100 K are shown in Figure 10. The spectra consist of a rhombic signal characteristic of a four-coordinate square-planar Ni^{III} (a d^7 low-spin system) with an $S = 1/2$ ground state. The individual g values for $[1^{\text{Ox}}]^+$ and $[2^{\text{Ox}}]^+$ are 2.360, 2.167, and 2.005 and 2.300, 2.225, and 2.008, while for the $[3^{\text{Ox}}]^+$ and $[4^{\text{Ox}}]^+$ are 2.310, 2.226, and 2.018, and 2.205, 2.188, and 2.006, respectively. The large rhombicity and the

high average g values ($g_{\text{avg}} = (g_1 + g_2 + g_3)/3$; 2.177, 2.178, 2.185, and 2.133, for $[1^{\text{Ox}}]^+$, $[2^{\text{Ox}}]^+$, $[3^{\text{Ox}}]^+$, $[4^{\text{Ox}}]^+$, respectively) unambiguously indicates that the oxidation is located on the Ni center, thereby confirming the Ni^{III} nature of the singly oxidized species.^[25] In case ligand oxidation had occurred, the resulting cation-radical would likely to exhibit an isotropic EPR spectrum with g value close to the free electron value of 2.002.^[25a,25b] Moreover, the presence of three distinct signals (g_1 , g_2 , and g_3) in the spectrum also rules out the existence of a 5- or 6-coordinate species in solution as that would give an axial signal with $g_{\perp} > g_{\parallel}$. In fact, the solution generated Ni^{III} species of the dioxo[14]-ane N_4 ligand displays g_{\perp} at 2.23 and g_{\parallel} at 2.02 with $g_{\perp} > g_{\parallel}$.^[28] These findings along with the absorption spectroscopic data strongly suggest that the present Ni complexes remain four-coordinated. The observation of the three different g values at 2.193, 2.080, and 2.006 for the Ni^{III} species reported by the Journaux and Garcia, are quite similar to the present systems, thus again indicating a similar electronic structure. In fact, these authors have suggested that the unpaired electron occupies a π -type metal 3d orbital and thus attesting the metal-centered oxidation rather than the ligand-centered oxidation.^[25c]

Our efforts to characterize the doubly oxidized species were unsuccessful owing to very unstable nature of the respective species. The electrochemical oxidation at the 2nd (for **2**, **3** and **4**) and 3rd potential (for **4** only) immediately lead to the decomposition of the transiently generated species. It is to be noted, however, that all these redox processes were $1e^-$ in nature as determined by the coulometry.

Chemical Oxidation and Vindication of Electrochemical Findings

The accessible redox potentials (cf. Table 4) of the complexes **1–4** and the successful electrochemical generation of the singly oxidized forms, $[1^{\text{Ox}}]^+ - [4^{\text{Ox}}]^+$, prompted us to try chemical oxidation. A number of $1e^-$ oxidants were attempted (for example, $(\text{NH}_4)_2[\text{Ce}(\text{NO}_3)_6]$, $[\text{NO}]\text{BF}_4$, and $\text{Ag}(\text{OTf})$,^[29] however, a mixture of species and decomposed products avoided the clear conversion, until a rather uncommon oxidant, $\text{Cu}(\text{OTf})_2$ was used. The redox potential of the $\text{Cu}(\text{OTf})_2$ in CH_3CN is 0.8 V vs. SCE^[29] and clearly seem to cause oxidation at the first oxidation potential of the complexes **1–4**. Indeed, addition of 1.2 equiv. of the $\text{Cu}(\text{OTf})_2$ to a CH_3CN solution of the respective Ni^{II} complex, resulted in a clean $1e^-$ oxidation. The chemical oxidation of the solution containing the respective Ni complex generated a green to greenish-brown species as observed electrochemically before. The UV/Vis spectra of the chemically oxidized form were recorded and found to be identical as shown in Figure 9. EPR spectra of the oxidized species were not attempted due to the possible contamination from the unreacted $\text{Cu}(\text{OTf})_2$.

Conclusions

The presented work demonstrates the syntheses and characterization of four novel square-planar Ni^{II} complexes

with amide-amine-based macrocyclic ligands. The important findings of the present study are summarized as follows:

- (1) To the best of our knowledge, for the first time a systematic investigation has been carried out to understand the structural, spectroscopic and redox properties of the Ni^{II} ion in a set of 12-membered macrocyclic ligands.
- (2) Crystal structures show a very tight binding of the Ni ion by the macrocyclic ligand in all four cases. Some of the $\text{Ni}-\text{N}_{\text{amide}}$ bond lengths are the shortest amongst the literature examples.
- (3) The occurrence of the geminal coupling for few protons in the proton NMR spectra clearly depict the inherent strain present in the macrocycle of the Ni^{II} complexes.
- (4) The low-valent Ni^{II} complexes are capable of undergoing one, two and in one case three $1e^-$ oxidations that are successively metal- and ligand-centered, as revealed by the trend observed in the formal redox potentials on changing the ligand along the present series of the complexes.
- (5) The Ni^{III} species were generated in solution both electrochemically and chemically [after oxidizing with $\text{Cu}(\text{OTf})_2$] and shown to have rich spectroscopic features.
- (6) The unstable $1e^-$ oxidized species are concluded to be Ni^{III} species by the absorption spectra and their anisotropic EPR spectra typical for a Ni^{III} ion in a square-planar geometry.
- (7) The $2e^-$ and $3e^-$ oxidations, which are ligand-centered, lead to immediate decomposition, and prevented us to characterize this species.

Experimental Section

Materials and Reagents: All reagents were obtained from commercial sources and used as received. N,N' -Dimethylformamide (DMF) was dried and distilled from 4-Å molecular sieves and stored over sieves. Acetonitrile (MeCN) was dried by distillation from anhydrous CaH_2 . Diethyl ether was dried by refluxing over sodium metal wires under inert atmosphere. Tetrahydrofuran (THF) was dried by refluxing and distilling from sodium metal and benzophenone. Ethyl alcohol ($\text{C}_2\text{H}_5\text{OH}$) and methyl alcohol (CH_3OH) were distilled from magnesium ethoxide and magnesium methoxide, respectively. Chloroform (CHCl_3) and dichloromethane (CH_2Cl_2) were purified by washing with 5% aqueous sodium carbonate solution followed by water and finally dried with anhydrous CaCl_2 , before a final reflux and distillation. Petroleum ether (boiling range: 60–80 °C) and hexanes (boiling range: 60–80 °C) were dried by refluxing and distilling over sodium metal wires. N,N' -bis(chloroacetyl)ethylenediamine and N,N' -bis(chloroacetyl)-*o*-phenylenediamine were prepared according to a published procedure.^[14]

Ligand Syntheses

$\text{H}_2\text{L}^{\text{EN}}$: LiBr (0.8 g, 9 mmol), Na_2CO_3 (4.0 g, 40 mmol) and N,N' -bis(chloroacetyl)ethylenediamine (1.0 g, 5 mmol) were taken in MeCN (140 mL) and the mixture was refluxed with stirring for 1 h. To this was added N,N' -dimethylethylenediamine (0.4 g, 5 mmol) dissolved in MeCN (20 mL). The resulting mixture was refluxed whilst stirring for an additional 48 h. The mixture was cooled, filtered and the solvent was removed under reduced pressure to afford a semi-mass. The crude product was further purified by column

chromatography using silica gel (100–200 mesh) with 10% MeOH/CHCl₃ (R_f = 0.45). A white product was obtained after purification. Yield 0.15 g (16%). An analytically pure product (in ca. 75% yield) can also be obtained by recrystallizing the crude product by layering the CHCl₃ solution with the petroleum ether (boiling range: 60–80 °C). C₁₀H₂₀N₄O₂ (228.30): calcd. C 52.61, H 8.83, N 24.54; found C 52.95, H 8.82, N 24.34. M.p. 170–174 °C. ¹H NMR (300 MHz, CDCl₃, 25 °C): δ = 2.38 (s, 6 H, CH₃), 2.50 (s, 4 H, –CH₂CH₂–), 2.96 [s, 4 H, –CH₂C(O)–], 3.48 (m, 4 H, –CH₂CH₂–), 7.2 [s (broad), 2 H, NH] ppm. FT-IR (KBr disk): $\tilde{\nu}$ = 3310, 2940, 2840, 2820, 2781, 1651 cm^{–1}. MS (EI⁺, m/z): calcd. for C₁₀H₂₀N₄O₂ 228.30, found 228.58.

H₂^{2EN}: This ligand was synthesized in a similar manner as that of H₂^{1EN} with following reagents: LiBr (0.51 g, 5.8 mmol), Na₂CO₃ (2.49 g, 23.52 mmol), *N,N'*-bis(chloroacetyl)ethylenediamine (0.63 g, 2.94 mmol), and *N,N'*-dimethyl-*o*-phenylenediamine (0.4 g, 2.94 mmol). The crude product was recrystallized by layering the CHCl₃ layer with hexanes. Yield 0.250 g (30%). C₁₄H₂₀N₄O₂ (277.34): calcd. C 60.85, H 7.30, N 20.28; found C 60.79, H 7.18, N 19.68. M.p. 164–165 °C. ¹H NMR (300 MHz, CDCl₃, 25 °C): δ = 2.85 (s, 6 H, CH₃), 2.78 (s, 4 H, –CH₂CH₂–), 3.56 [s, 4 H, –CH₂C(O)–], 7.2–7.4 (m, 4 H, arom.), 9.5 [s (broad), 2 H, NH] ppm. FT-IR (KBr disk): $\tilde{\nu}$ = 3233, 3050, 2866, 1664 cm^{–1}. MS (EI⁺, m/z): calcd. for C₁₄H₂₀N₄O₂ 277.34, found 277.344.

H₂^{3OP}: This ligand was synthesized in a similar manner as that of H₂^{1EN}. However, this time following reagents were used: LiBr (0.7 g, 8 mmol), Na₂CO₃ (4.0 g, 32 mmol), *N,N'*-bis(chloroacetyl)-*o*-phenylenediamine (1.0 g, 4 mmol), and *N,N'*-dimethylethylenediamine (0.4 g, 4 mmol). The crude product was recrystallized from CHCl₃ solution after layering with the petroleum ether (boiling range: 60–80 °C). Yield 0.90 g (95%). C₁₄H₂₀N₄O₂ (276.34): calcd. C 60.85, H 7.30, N 20.28; found C 60.49, H 7.42, N 20.61. M.p. 164–165 °C. ¹H NMR (300 MHz, CDCl₃, 25 °C): δ = 2.45 (s, 6 H, CH₃), 2.64 (m, 4 H, –CH₂CH₂–), 3.16 [s, 4 H, –CH₂C(O)–], 7.21 (m, 2 H, arom.), 7.60 (m, 2 H, arom.), 9.48 [s (broad), 2 H, NH] ppm. FT-IR (KBr disk): $\tilde{\nu}$ = 3221, 2942, 2833, 1674 cm^{–1}. MS (EI⁺, m/z): calcd. for C₁₄H₂₀N₄O₂ 276.34, found 276.38.

H₂^{4OP}: Using the aforementioned procedure, the ligand H₂^{4OP}, was synthesized with following reagents: LiBr (1.3 g, 14.8 mmol), Na₂CO₃ (6.3 g, 59 mmol), *N,N'*-bis(chloroacetyl)-*o*-phenylenediamine (1.93 g, 7.4 mmol), and *N,N'*-dimethyl-*o*-phenylenediamine (1.0 g, 7.4 mmol). The crude product was recrystallized from CHCl₃ solution after layering with the petroleum ether (boiling range: 60–80 °C) or hexanes. Yield 1.0 g (42%). C₁₈H₂₀N₄O₂ (324.38): calcd. C 66.65, H 6.21, N 17.27; found C 66.7, H 6.15, N 16.98. M.p. 178–184 °C. ¹H NMR (300 MHz, CDCl₃, 25 °C): δ = 2.95 (s, 6 H, CH₃), 3.72 [s, 4 H, –CH₂C(O)–], 7.12 (m, 4 H, arom.), 7.22 (m, 4 H, arom.), 7.52 [s (broad), 2 H, NH] ppm. FT-IR (KBr disk): $\tilde{\nu}$ = 3317, 3221, 2942, 2833, 1689 cm^{–1}. MS (EI⁺, m/z): calcd. for C₁₈H₂₀N₄O₂ 324.38, found 324.60.

Syntheses of Metal Complexes

[Ni^{II}(^{1EN})] (1) Method A: The ligand H₂^{1EN} (0.10 g, 0.44 mmol) was dissolved in DMF (10 mL) under magnetic stirring and solid NaH (0.023 g, 0.96 mmol) was added under nitrogen atmosphere. The resulting mixture was stirred until H₂ evolution was ceased. To this mixture was added a solution of NiCl₂ (0.057 g, 0.44 mmol) dissolved in DMF (5 mL). The resulting deep yellow solution was stirred for 3 h at room temperature. The solvent was evaporated under reduced pressure and the crude compound was isolated after washing with diethyl ether. The crude compound was dissolved in MeCN (15 mL) and passed through celite pad in a medium porosity frit. The filtrate was concentrated to 1/3rd of its original volume

and the diffusion of diethyl ether resulted in deep yellow crystalline product in a day. The product was filtered and dried under vacuum. Yield 0.040 g (35%).

Method B: The ligand H₂^{1EN} (0.10 g, 0.439 mmol) was dissolved in MeOH (5 mL) and treated with solid NaOH (0.035 g, 0.88 mmol) under magnetic stirring. A solution of Ni(OAc)₂ dissolved in MeOH (6 mL) was added dropwise to the ligand solution. The resulting straw yellow solution was stirred for 2 h at room temperature. The solvent was removed under reduced pressure and the crude compound was isolated after washing with diethyl ether. The recrystallization was achieved by dissolving the crude compound in MeCN and diffusing diethyl ether. The highly crystalline deep yellow product was filtered, washed with diethyl ether and dried under vacuum. Yield 0.050 g (40%). C₁₀H_{18.5}N₄O_{2.25}Ni (including 0.25H₂O, 284.97): calcd. C 41.49, H 6.40, N 19.36; found C 41.56, H 6.39, N 19.03. FT-IR (KBr disk): $\tilde{\nu}$ = 3400, 2984, 2948, 2905, 2859, 2808, 1607 cm^{–1}. Conductivity (CH₃CN, ca. 1 mM solution, 298 K): Λ_M = 2 Ω^{-1} cm² mol^{–1}. UV/Vis [λ_{max} , nm (ϵ , M^{–1} cm^{–1})] (in CH₃CN): 230 sh (18200), 260 sh (6100), 436 (390). UV/Vis [λ_{max} , nm (ϵ , M^{–1} cm^{–1})] (in DMF): 440 (400). UV/Vis [λ_{max} , nm (ϵ , M^{–1} cm^{–1})] (in DMSO): 440 (570). UV/Vis [λ_{max} , nm (ϵ , M^{–1} cm^{–1})] (in H₂O): 435 (140). MS (EI⁺, m/z): calcd. for C₁₀H_{18.5}N₄O_{2.25}Ni 284.08, found 285.05 (1 + H⁺). ¹H NMR ([D₆]DMSO, 300 MHz, 25 °C): δ = 2.49 (s, 6 H, –CH₃), 2.67 (m, 4 H, –CH₂–), 3.07 (d, 2 H, –CH₂C(O)–), 3.21 (m, 2 H, –CH₂–), 3.76 (m, 2 H, –CH₂–), 4.00 (d, 2 H, –CH₂C(O)–) ppm. ¹H NMR (CD₃CN, 300 MHz, 25 °C): δ = 2.45 (s, 6 H, –CH₃), 2.66 (m, 4 H, –CH₂–), 3.08 (d, 2 H, –CH₂C(O)–), 3.25 (m, 2 H, –CH₂–), 3.69 (m, 2 H, –CH₂–), 3.90 (d, 2 H, –CH₂C(O)–) ppm. ¹³C NMR ([D₆]DMSO, 300 MHz, 25 °C): δ = 48.21 (–CH₃), 49.07 (–CH₂CH₂–), 60.70 (–CH₂CH₂–), 69.66 (–C(O)CH₂–), 175.14 (C=O) ppm.

[Ni^{II}(^{2EN})] (2): This complex was synthesized following the method A (yield 45%) or B (yield 35%) for complex 1. C₁₄H₁₉N₄O_{2.5}Ni (including 0.5H₂O, 333.01): calcd. C 46.70, H 5.83, N 15.56; found C 46.51, H 5.83, N 15.32. FT-IR (KBr disk): $\tilde{\nu}$ = 3400, 2935, 2866, 1598 cm^{–1}. Conductivity (CH₃CN, ca. 1 mM solution, 298 K): Λ_M = 12 Ω^{-1} cm² mol^{–1}. UV/Vis [λ_{max} , nm (ϵ , M^{–1} cm^{–1})] (in CH₃CN): 241 (7560), 440 (270). UV/Vis [λ_{max} , nm (ϵ , M^{–1} cm^{–1})] (in DMF): 440 (270). UV/Vis [λ_{max} , nm (ϵ , M^{–1} cm^{–1})] (in DMSO): 438 (200). UV/Vis [λ_{max} , nm (ϵ , M^{–1} cm^{–1})] (in H₂O): 430 (190). MS (EI⁺, m/z): calcd. for C₁₄H₁₈N₄O₂Ni 332.08, found 333.27 (2 + H⁺). ¹H NMR ([D₆]DMSO, 300 MHz, 25 °C): δ = 2.78 (m, 2 H, –CH₂–), 2.87 (s, 6 H, –CH₃), 3.22 (m, 2 H, –CH₂–), 3.70 (d, 2 H, –CH₂C(O)–), 4.15 (d, 2 H, –CH₂C(O)–), 7.47 (m, 4 H, arom. H) ppm. ¹H NMR (CD₃CN, 300 MHz, 25 °C): δ = 2.73 (m, 2 H, –CH₂–), 2.79 (s, 6 H, –CH₃), 3.23 (m, 2 H, –CH₂–), 3.58 (d, 2 H, –CH₂C(O)–), 4.13 (d, 2 H, –CH₂C(O)–), 7.26 (m, 2 H, arom. H), 7.36 (m, 2 H, arom. H) ppm. ¹³C NMR ([D₆]DMSO, 300 MHz, 25 °C): δ = 48.23 (–CH₃), 51.34 (–CH₂CH₂–), 70.03 (–C(O)CH₂–), 123.75 (Ar-h), 129.83 (Ar-g), 149.14 (Ar-f), 172.47 (C=O) ppm.

[Ni^{II}(^{3OP})] (3): A similar procedure as that of 1 was followed and the product was isolated as deep yellow blocks. Yield from method A: 42%. Yield from method B: 37%. C₁₄H₁₈N₄O₂Ni (333.01): calcd. C 50.50, H 5.41, N 16.83; found C 50.53, H 5.33, N 16.62. FT-IR (KBr disk): $\tilde{\nu}$ = 2933, 1619, 1601 cm^{–1}. Conductivity (CH₃CN, ca. 1 mM solution, 298 K): Λ_M = 10 Ω^{-1} cm² mol^{–1}. UV/Vis [λ_{max} , nm (ϵ , M^{–1} cm^{–1})] (in CH₃CN): 271 (1300), 291 (11360), 444 (325). UV/Vis [λ_{max} , nm (ϵ , M^{–1} cm^{–1})] (in DMF): 292 (18200), 441 (370). UV/Vis [λ_{max} , nm (ϵ , M^{–1} cm^{–1})] (in DMSO): 441 (250). UV/Vis [λ_{max} , nm (ϵ , M^{–1} cm^{–1})] (in H₂O): 437 (350). MS (EI⁺, m/z): calcd. for C₁₄H₁₈N₄O₂Ni 332.08, found 333.06 (3 + H⁺). ¹H NMR ([D₆]DMSO, 300 MHz, 25 °C): δ = 2.52 (s, 6H –CH₃), 2.74 (m, 2

H, $-\text{CH}_2-$), 3.12 (d, 2 H, $-\text{CH}_2\text{C}(\text{O})-$), 3.86 (m, 2 H, $-\text{CH}_2-$), 4.13 (d, 2 H, $-\text{CH}_2\text{C}(\text{O})-$), 6.54 (m, 2 H, Ar-g), 7.41 (m, 2 H, Ar-f) ppm. ^1H NMR (CD_3CN , 300 MHz, 25°C): δ = 2.64 (s, 6H $-\text{CH}_3$), 2.80 (m, 2 H, $-\text{CH}_2-$), 3.28 (d, 2 H, $-\text{CH}_2\text{C}(\text{O})-$), 3.89 (m, 2 H, $-\text{CH}_2-$), 4.14 (d, 2 H, $-\text{CH}_2\text{C}(\text{O})-$), 6.70 (m, 2 H, Ar-g), 7.56 (m, 2 H, Ar-f) ppm. ^{13}C NMR ($[\text{D}_6]\text{DMSO}$, 300 MHz, 25°C): δ = 47.68 ($-\text{CH}_3$), 59.72 ($-\text{CH}_2\text{CH}_2-$), 69.50 ($-\text{C}(\text{O})\text{CH}_2-$), 119.15 (Ar-k), 120.30 (Ar-j), 142.36 (Ar-i), 171.60 ($\text{C}=\text{O}$) ppm.

[Ni^{II}(4^{OP})] (4): This complex was also synthesized in an analogous method and the recrystallized product was isolated as orange-yellow crystals in 38% from method A and 30% from method B. $\text{C}_{18}\text{H}_{18}\text{N}_4\text{O}_2\text{Ni}$ (380.69): calcd. C 56.79, H 4.77, N 14.7; found C 56.78, H 4.85, N 14.63. FT-IR (KBr disk): $\tilde{\nu}$ = 3006, 2935, 1632 cm^{-1} . Conductivity (CH_3CN , ca. 1 mM solution, 298 K): Λ_{M} = $2\ \Omega^{-1}\text{cm}^2\text{mol}^{-1}$. UV/Vis [λ_{max} , nm (ϵ , $\text{M}^{-1}\text{cm}^{-1}$)] (in CH_3CN): 265 (17000), 290 (13000), 443 (250). UV/Vis [λ_{max} , nm (ϵ , $\text{M}^{-1}\text{cm}^{-1}$)] (in DMF): 291 (10600), 441 (200). UV/Vis [λ_{max} , nm (ϵ , $\text{M}^{-1}\text{cm}^{-1}$)] (in DMSO): 441 (250). UV/Vis [λ_{max} , nm, qualitative (in H_2O)]: 438. MS (EI^+ , m/z): calcd. for $\text{C}_{18}\text{H}_{18}\text{N}_4\text{O}_2\text{Ni}$ 380.08, found 381.35 ($4 + \text{H}^+$). ^1H NMR (CD_3CN , 300 MHz, 25°C): δ = 3.00 (s, 6 H, $-\text{CH}_3$), 3.80 (d, 2 H, $-\text{CH}_2\text{C}(\text{O})-$), 4.42 (d, 2 H, $-\text{CH}_2\text{C}(\text{O})-$), 6.65 (m, 2 H, Ar-i), 7.30 (m, 2 H, Ar-h), 7.44 (m, 2 H, Ar-g), 7.62 (m, 2 H, Ar-f) ppm. ^1H NMR ($[\text{D}_6]\text{DMSO}$, 300 MHz, 25°C): δ = 3.01 (s, 6 H, $-\text{CH}_3$), 3.89 (d, 2 H, $-\text{CH}_2\text{C}(\text{O})-$), 4.43 (d, 2 H, $-\text{CH}_2\text{C}(\text{O})-$), 6.67 (m, 4 H, Ar-H), 7.55 (m, 4 H, Ar-H) ppm. ^1H NMR (CDCl_3 , 300 MHz, 25°C): δ = 3.06 (s, 6 H, $-\text{CH}_3$), 3.86 (d, 2 H, $-\text{CH}_2\text{C}(\text{O})-$), 4.51 (d, 2 H, $-\text{CH}_2\text{C}(\text{O})-$), 6.85 (m, 2 H, Ar-i), 7.25 (m, 2 H, Ar-h), 7.49 (m, 2 H, Ar-g), 7.76 (m, 2 H, Ar-f) ppm. ^{13}C NMR ($[\text{D}_6]\text{DMSO}$, 300 MHz, 25°C): δ = 51.81 ($-\text{CH}_3$), 70.33 ($-\text{C}(\text{O})\text{CH}_2-$), 119.41 (Ar-k), 121.09 (Ar-j), 123.59 (Ar-h), 129.94 (Ar-g), 142.46 (Ar-i), 148.81 (Ar-f), 170.63 ($\text{C}=\text{O}$) ppm.

Physical Measurements: The conductivity measurements were done in organic solvents using the digital conductivity bridge from Popular Traders, India (model number: PT-825). The elemental analysis data were obtained from Elementar Analysen Systeme GmbH Vario EL-III instrument. The NMR measurements were done using either Hitachi R-600 FT NMR (60 MHz) or an Avance Bruker (300 MHz) instrument. The infra-red spectra (either as KBr pellet or as a mull in mineral oil) were recorded using the Perkin-Elmer FTIR 2000 spectrometer. The absorption spectra were recorded using the Perkin-Elmer Lambda-25 spectrophotometer. The mass spectra were obtained on a Jeol SX102/DA-6000 instrument.

Electrochemical Measurements: Cyclic voltammetric experiments were performed by using a PAR model 370 electrochemistry system consisting of M-174A polarographic analyzer, M-175 universal programmer, and RE 0074 X-Y recorder or a CH instruments electrochemical analyzer (Model No. 600B Series). The cell contained a glassy carbon (PAR model G0021) or a Beckman Pt (M-39273) working electrode, a Pt wire auxiliary electrode, and a saturated calomel electrode (SCE) as reference electrode. A salt bridge (containing supporting electrolyte, tetra-*n*-butylammonium perchlorate (TBAP) dissolved in either MeCN or DMF) was used to connect the SCE with the electrochemistry solution.^[30] For constant potential electrolysis experiments a Pt-mesh was used as the working electrode. The solutions were ca. 1 mM in complex and ca. 0.1 M in supporting electrolyte, tetra-*n*-butylammonium perchlorate (TBAP). Under our experimental conditions, the $E_{1/2}$ values (in Volts) for the couple Fc^+/Fc were 0.40 in MeCN vs. SCE.

Crystal Structure Determination: X-ray diffraction studies of crystal mounted on a capillary were carried out on a Bruker AXS SMART-APEX diffractometer with a CCD area detector (K_α radiation, λ = 0.71073 Å, monochromator: graphite).^[31] Frames were

collected at T = 293 as well as at T = 100 K by ω , ϕ and 2θ rotation at 10 s per frame with SAINT.^[32] The measured intensities were reduced to F^2 and corrected for absorption with SADABS.^[33] Structure solution, refinement, and data output were carried out with the SHELXTL program.^[33] Non-hydrogen atoms were refined anisotropically. All hydrogen atoms were placed in geometrically calculated positions by using a riding model. For complex 3, disorder was observed for the C6 and C7 atoms of the amine fragment. These atoms (C6 and C7) were occupying two crystallographically independent positions which could be located from the additional residual electron density. The site occupancy factors were refined with the help of free variable PART instruction. Refinement of the site occupancy factors (SOFs) for the disordered atoms C6 and C7 gave the value 0.81 (2) this factor was thereafter fixed at 0.80. The occupancy factor of the other possible set of positions (C6D/C7D) was 0.20. A structure model based on a statistically disordered C atom improved the accuracy of C–C bonds of interest. H atoms have been omitted from the disordered part. Table 1 contains necessary crystallographic details.

CCDC-635113 to -635116 (for 1–4) contain the supplementary crystallographic data for this paper. These data can be obtained free of charge from The Cambridge Crystallographic Data Centre via www.ccdc.cam.ac.uk/data_request/cif.

Supporting Information (see also the footnote on the first page of this article): Crystal packing diagram of complex 2 (Figure S1); lateral view of the crystal structures of the complexes 1, 2, 3, and 4 (Figure S2); absorption spectra for complexes 1, 2, 3, and 4 recorded in DMF (Figure S3), DMSO (Figure S4), and H_2O (Figure S5); ^1H NMR spectra of complexes 1, 2, 3, and 4 in $[\text{D}_3]\text{MeCN}$ (Figure S6) and in $[\text{D}_6]\text{DMSO}$ (Figure S7), ^1H NMR spectra of complex 4 in CDCl_3 (Figure S8) and ^{13}C NMR spectra of complexes 1, 2, 3, and 4 in $[\text{D}_6]\text{DMSO}$ (Figure S9); 2D $\{^1\text{H}-^{13}\text{C}\}$ NMR spectrum of complex 1 (Figure S10); Plane and displacement parameters (Table S1); and ^{13}C NMR spectroscopic data (Table S2).

Acknowledgments

Authors (RG) thank the Department of Science and Technology (DST), New Delhi, India for the financial support, Professors R. Ramanan and A. K. Ganguli from Indian Institute of Technology, New Delhi, India for the crystallographic help, and DST-FIST funded single crystal diffraction facility at IIT-Delhi for data collection. We express our deepest gratitude to Professor R. Mukherjee and his research group at IIT - Kanpur for extending their laboratory facilities for the detailed electrochemical studies. Reviewer's suggestions during the revision stage were very helpful.

- [1] a) J. D. Koola, J. K. Kochi, *Inorg. Chem.* **1987**, 26, 908; b) H. Yoon, C. J. Burrows, *J. Am. Chem. Soc.* **1988**, 110, 4087; c) T. R. Wagler, C. J. Burrows, *Tetrahedron Lett.* **1988**, 29, 5091; d) B. Dangel, M. Clarke, J. Haley, D. Sames, R. Polt, *J. Am. Chem. Soc.* **1997**, 119, 10865; e) T. R. Wagler, Y. Fang, C. J. Burrows, *J. Org. Chem.* **1989**, 54, 1584.
- [2] a) R. Cammack, *Adv. Inorg. Chem.* **1988**, 32, 297; b) J. J. G. Moura, I. Moura, M. Teixeira, A. V. Xavier, G. D. Fauque, J. Legall, *Met. Ions Biol. Syst.* **1988**, 23, 285.
- [3] H.-D. Youn, E.-J. Kim, J.-H. Roe, Y. C. Hah, S.-O. Kang, *Biochem. J.* **1996**, 318, 889.
- [4] P. A. Lindahl, *Biochemistry* **2002**, 41, 2097.
- [5] U. Ermler, W. Grabarse, S. Shima, M. Goubeaud, R. K. Thauer, *Science* **1997**, 278, 1457.
- [6] a) M. L. Golden, M. V. Rampersad, J. H. Reibenspies, M. Y. Darensbourg, *Chem. Commun.* **2003**, 1824; b) Q. Wang, A. J.

- Blake, E. S. Davies, E. J. L. McInnes, C. Wilson, M. Schroder, *Chem. Commun.* **2003**, 3012; c) R. Krishnan, J. K. Voo, C. G. Riordan, L. Zahkarov, A. L. Rheingold, *J. Am. Chem. Soc.* **2003**, *125*, 4422; d) R. C. Linck, C. W. Spahn, T. B. Rauchfuss, S. R. Wilson, *J. Am. Chem. Soc.* **2003**, *125*, 8700; e) R. Krishnan, C. G. Riordan, *J. Am. Chem. Soc.* **2004**, *126*, 4484; f) T. C. Harrop, M. M. Olmstead, P. K. Mascharak, *Chem. Commun.* **2004**, 1744; g) T. C. Harrop, M. M. Olmstead, P. K. Mascharak, *J. Am. Chem. Soc.* **2004**, *126*, 14714.
- [7] a) E. C. Long, *Acc. Chem. Res.* **1999**, *32*, 827; b) C. Harford, S. Narindrasorasak, B. Sarkar, *Biochemistry* **1996**, *35*, 4271.
- [8] E. Kimura, *J. Coord. Chem.* **1986**, *15*, 1 and references cited therein.
- [9] a) G. D. Santis, L. Fabbri, M. Licchelli, P. Pallavicini, *Coord. Chem. Rev.* **1992**, *120*, 237; b) D. W. Margerum, G. D. Owens, in *Metal Ions in Biological Systems*, Ed. H. Sigel, M. Dekker, New York, **1981**, *12*, 75; c) J. S. Rybka, D. W. Margerum, *Inorg. Chem.* **1980**, *19*, 2784; d) P. K. Mascharak, *Coord. Chem. Rev.* **2002**, *225*, 201; e) D. S. Marlin, M. M. Olmstead, P. K. Mascharak, *Inorg. Chem.* **1999**, *38*, 3258; f) F. A. Chavez, M. M. Olmstead, P. K. Mascharak, *Inorg. Chem.* **1997**, *36*, 6323; g) T. J. Collins, R. D. Powell, C. Slebocknick, E. S. Uffelman, *J. Am. Chem. Soc.* **1991**, *113*, 8419; h) J. M. Workman, R. D. Powell, A. D. Procyk, T. J. Collins, D. F. Bocian, *Inorg. Chem.* **1992**, *31*, 1548; i) L. Fabbri, *Comments Inorg. Chem.* **1985**, *4*, 33; j) L. Fabbri, T. A. Kaden, A. Perotti, B. Seghi, L. Siegfried, *Inorg. Chem.* **1986**, *25*, 321; k) R. W. Hay, P. R. Norman, *Transition Met. Chem.* **1980**, *5*, 232; l) R. W. Hay, R. Bembi, W. Sommerville, *Inorg. Chim. Acta* **1982**, *59*, 147; m) R. W. Hay, M. P. Pujari, F. McLaren, *Inorg. Chem.* **1984**, *23*, 3033.
- [10] a) M. Kodama, T. Yatsunami, E. Kimura, *J. Chem. Soc. Dalton Trans.* **1979**, 1783; b) M. Kodama, E. Kimura, *J. Chem. Soc. Dalton Trans.* **1981**, 694; c) E. Kimura, A. Sakonaka, R. Machida, *J. Am. Chem. Soc.* **1982**, *104*, 4255; d) E. Kimura, T. Koike, R. Machida, R. Nagai, M. Kodama, *Inorg. Chem.* **1984**, *23*, 4181; e) X. H. Bu, D. L. An, X. C. Cao, Y. T. Chen, M. Shionoya, E. Kimura, *Polyhedron* **1996**, *15*, 161; f) X. H. Bu, X. C. Cao, Z. H. Zhang, Z. A. Zhu, Y. T. Chen, M. Shionoya, E. Kimura, *Polyhedron* **1996**, *15*, 1203; g) X. H. Bu, D. L. An, Z. A. Zhu, Y. T. Chen, M. Shionoya, E. Kimura, *Polyhedron* **1997**, *16*, 179.
- [11] Y. D. Lampeka, S. P. Gavrich, R. W. Hay, T. Eisenblatter, P. Lightfoot, *J. Chem. Soc. Dalton Trans.* **2000**, 2023.
- [12] S. P. Gavrich, Y. D. Lampeka, P. Lightfoot, *Inorg. Chim. Acta* **2004**, *357*, 1023.
- [13] a) D. Kong, X. Ouyang, A. E. Martell, A. Clearfield, *Inorg. Chem. Commun.* **2003**, *6*, 317; b) J. Gao, J. H. Reibenspies, Y. Sun, A. E. Martell, *Helv. Chim. Acta* **2003**, *86*, 563.
- [14] H.-J. Krugar, G. Peng, R. H. Holm, *Inorg. Chem.* **1991**, *30*, 734.
- [15] A. Grenz, S. Ceccarelli, C. Bolm, *Chem. Commun.* **2001**, 1726.
- [16] J. W. Steed, J. L. Atwood, in *Supramolecular Chemistry*, John Wiley & Sons Ltd., **2000**, chapter 3.
- [17] K. Nakamoto in *Infrared and Raman Spectra of Inorganic and Coordination Compounds*, John Wiley & Sons, **1986**.
- [18] W. J. Geary, *Coord. Chem. Rev.* **1971**, *7*, 81.
- [19] P. Comba, S. P. Gavrich, R. W. Hay, P. Hilfenhaus, Y. D. Lampeka, P. Lightfoot, A. Peters, *Inorg. Chem.* **1999**, *38*, 1416.
- [20] T. J. Collins, T. R. Nichols, E. S. Uffelman, *J. Am. Chem. Soc.* **1991**, *113*, 4708.
- [21] L. Fabbri, *J. Chem. Soc. Dalton Trans.* **1979**, 1857.
- [22] a) M. Ray, D. Ghosh, Z. Shirin, R. Mukherjee, *Inorg. Chem.* **1997**, *36*, 3568; b) A. K. Patra, R. Mukherjee, *Inorg. Chem.* **1999**, *38*, 1388; c) A. K. Patra, M. Ray, R. Mukherjee, *Inorg. Chem.* **2000**, *39*, 652; d) A. K. Singh, R. Mukherjee, *Dalton Trans.* **2005**, 2886.
- [23] a) M. Ray, S. Mukherjee, R. Mukherjee, *J. Chem. Soc. Dalton Trans.* **1990**, 3635; b) M. Ray, R. Mukherjee, *Polyhedron* **1992**, *11*, 2929.
- [24] a) C.-M. Che, W.-H. Leung, C.-K. Li, H.-Y. Cheng, S.-M. Peng, *Inorg. Chim. Acta* **1992**, *196*, 43; b) S.-T. Mak, V. W.-W. Yam, C.-M. Che, T. C. W. Mak, *J. Chem. Soc. Dalton Trans.* **1990**, 2555; c) W.-H. Leung, J.-X. Ma, V. W.-W. Yam, C.-M. Che, C.-K. Poon, *J. Chem. Soc. Dalton Trans.* **1991**, 1071; d) S.-T. Mak, W.-T. Wong, V. W.-W. Yam, T.-F. Lai, C.-M. Che, *J. Chem. Soc. Dalton Trans.* **1991**, 1915; e) T. J. Collins, D. R. Powell, C. Slebocknick, E. S. Uffelman, *J. Am. Chem. Soc.* **1991**, *113*, 8419; f) S.-M. Peng, C.-T. Chen, D.-S. Liaw, C.-I. Chen, Y. Wang, *Inorg. Chim. Acta* **1985**, *101*, L31; g) S.-M. Peng, D.-S. Liaw, *Inorg. Chim. Acta* **1986**, *113*, L11.
- [25] a) A. Aukauloo, X. Ottenwaelder, R. Ruiz, S. Poussereau, Y. Pei, Y. Journaux, P. Fleurat, F. Volatron, B. Cervera, M. C. Munoz, *Eur. J. Inorg. Chem.* **1999**, 1067; b) X. Ottenwaelder, R. Ruiz, R. Ruiz-Garcia, G. Blondin, R. Carasco, J. Cano, D. Lexa, Y. Journaux, A. Aukauloo, *Chem. Commun.* **2004**, 504; c) X. Ottenwaelder, A. Aukauloo, Y. Journaux, R. Carasco, J. Cano, B. Cervera, I. Castro, S. Curreli, M. C. Munoz, A. L. Rosello, B. Soto, R. Ruiz-Garcia, *Dalton Trans.* **2005**, 2516; d) R. Carasco, J. Cano, X. Ottenwaelder, A. Aukauloo, Y. Journaux, R. Ruiz-Garcia, *Dalton Trans.* **2005**, 2527.
- [26] a) R. Ruiz, C. S. Barland, A. Aukauloo, E. Anxolabehere-Mallart, Y. Journaux, J. Cano, M. C. Munoz, *J. Chem. Soc. Dalton Trans.* **1997**, 745; b) B. Cervera, J. L. Sanz, M. J. Ibanez, G. Vila, F. Lloret, M. Julve, R. Ruiz, X. Ottenwaelder, A. Aukauloo, S. Poussereau, Y. Journaux, M. C. Munoz, *J. Chem. Soc. Dalton Trans.* **1998**, 781.
- [27] Y. D. Lampeka, S. P. Gavrich, *Polyhedron* **2000**, *19*, 2533.
- [28] L. Fabbri, A. Poggi, *J. Chem. Soc. Chem. Commun.* **1980**, 646.
- [29] N. G. Connelly, W. E. Geiger, *Chem. Rev.* **1996**, *96*, 877.
- [30] D. T. Sawyer, J. L. Roberts Jr, *Experimental Electrochemistry for Chemists*, Wiley, New York, 1974.
- [31] SMART: Bruker Molecular Analysis Research Tool, Version 5.618, Bruker Analytical X-ray Systems, **2000**.
- [32] SAINT-NT, Version 6.04, Bruker Analytical X-ray Systems, **2001**.
- [33] SHELXTL-NT, Version 6.10, Bruker Analytical X-ray Systems, **2000**.

Received: January 30, 2007
Published Online: May 29, 2007